COMPARISON BETWEEN JOHNSON COOK'S PLASTICITY WITH DAMAGE MODEL AND ISOTROPIC HARDENING PLASTICITY WITH DUCTILE DAMAGE MODEL ON ALUMINIUM ALLOY SHEET 2024 T3 TENSILE TEST IN CORRELATING THE FINITE ELEMENT METHOD (FEM) TO THE EXPERIMENT TEST RESULT

Henry Gunsalam[1], Ahmad Sufian Abdullah[1,2*], Murni Awi[1], Mohd Rozaiman Aziz[1] and Kamarul-Azhar Kamarudin[3]

[1] Mechanical Engineering Studies, College of Engineering, Universiti Teknologi MARA, Cawangan Pulau Pinang, Kampus Permatang Pauh, Penang, Malaysia.

[2] Advanced Mechanics Research Group, Mechanical Engineering Studies, College of Engineering, Universiti Teknologi MARA, Cawangan Pulau Pinang, Kampus Permatang Pauh, Penang, Malaysia.

[3] Crashworthiness and Collisions Research Group (COLORED), Faculty of Mechanical and Manufacturing Engineering, Universiti Tun Hussein Onn Malaysia, Batu Pahat, 86400, Malaysia.

[*]Corresponding email: ahmadsufian@uitm.edu.my

Article history
Received
24th February2023
Revised
9th September 2023
Accepted
5th November 2023
Published
1st December 2023

ABSTRACT

Sometimes students and/or researchers are faced with a limited sample and data issue and need to choose carefully which approaches to be used, especially in performing analysis with numerical analysis. As there are a lot of numerical analysis approaches that are having similar purposes and the approaches can be used depending on the analysis cases and objectives. For example, Johnson Cook's plasticity model and isotropic plasticity hardening model are the common approaches available and used in ABAQUS software to determine the metal and metal alloy plasticity or inelastic mechanical properties. Therefore, in this paper, two approaches – Johnson Cook's plasticity with damage model and isotropic plasticity hardening with ductile damage model which is used to define the metal and metal alloy mechanical properties and performance are studied using ABAQUS Computer Aided Engineering (CAE) software and compared accordingly. In this study, the experimental result of the tensile test was used to determine the mechanical properties of the Aluminium alloy 2024 T3 sheet with 0.29mm thickness. Then the experiment test data are used to correlate the finite element method (FEM) model and the experimental test result by using Johnson Cook's plasticity hardening with damage model approach and the isotropic hardening plasticity with ductile damage model approach. Based on the comparison with the experiment failure sample mode, both FEM model failure mode is closely identical to the experiment failure sample. From the mechanical properties comparison, Johnson Cook's model shows a bigger deviation compared to the isotropic plasticity with ductile damage model in comparison to the experiment value. From this paper, it can be concluded that the ductile damage model is more appropriate to be used when the sample and data are limited.

Keywords: *Johnson Cook's hardening plasticity, Johnson Cook's damage model, Isotropic hardening plasticity, Ductile damage model, tensile experiment.*

 DOI: https://doi.org/10.11113/jm.v46.494

1.0 INTRODUCTION

In determining the material performances and properties, experimental methods are often used but with a high cost. As stated by Ahmad S.A *et all* [1], numerical analysis or finite element analysis can be implemented as it is a more cost-efficient investigation method [1]. Sometimes, we as students and researchers are faced with a limited sample and data issue and need to choose carefully which numerical analysis approaches to be used. As there are a lot of numerical analysis approaches that are having similar purposes and the approaches can be used depending on the analysis cases and objectives. For example, Johnson Cook's plasticity model, and isotropic plasticity hardening model are the common approaches available and used in ABAQUS software to determine the metal and alloy plasticity or inelastic mechanical properties. Ahmad S.A, et al. [1], Shuaishuai Y. et. al., [2], Zhang D. N. et al., [3], Sachin G., et. al [4], Tan J. Q., et. al [5], Sohail A., et. al. [6], Li S.Y., et. al. [7], Corona, et.al [8], Rasaee S. et. al. [9], Kay, G. [10], Shen W. J. et. al [11], Wang, C. et. al. [12], Bal B. et al. [13], Sonika S., et. al, [14], Meng X.X., et.al. [15] and a lot of more are using Johnson Cook's model to define and modelling the Aluminium alloy properties. Meanwhile, Børvik T. et. al [16], Ivaylo N.V. et. al [17], Asle J.T., et. al [18], Fribourg G., et.al.[19], Ole R. M., et. al [20], Abir B. et. al [21] and a few more are using isotropic plastic hardening in modeling and defining the Aluminium and Aluminium alloy properties.

Therefore, in this paper, two approaches Johnson Cook's plasticity with damage model and isotropic plasticity hardening with ductile damage model which is used to define the metal and alloy mechanical properties and performance are studied using ABAQUS Computer Aided Engineering (CAE) software and compared accordingly. The experimental result of the tensile test is used to determine the mechanical properties of the Aluminium alloy 2024 T3 sheet with 0.29mm thickness together with Johnson Cook model properties, isotropic plastic hardening properties and ductile damage properties. Then the mechanical properties data are used to correlate the finite element method (FEM) model and the experimental test result by using Johnson Cook's plasticity hardening with damage model approach and the isotropic hardening plasticity with ductile damage model approach. FEM results from the two models were compared with experimental results to determine which FEM model is appropriate to be used when the experiment sample and data are limited.

2.0 METHODOLOGY

2.1 Understanding the plasticity and failure/damage model

2.1.1 Johnson Cook's plasticity and failure/damage model

Johnson-Cook plasticity model is a particular type of Mises plasticity model with analytical forms of the hardening law and rate dependence. It is a particular type of isotropic hardening where the static yield stress, σ^0, is assumed to be of the form in Equation 1 [22],

$$\sigma^0 = \left[A + B\left(\bar{\varepsilon}^{pl}\right)^n\right]\left(1 - \hat{\theta}^m\right) \tag{1}$$

where $\bar{\varepsilon}^{pl}$ is the equivalent plastic strain and A (Yield stress), B (Strain hardening modulus), n (Strain hardening exponent) and m (temperature factor exponent) are material parameters measured at or below the transition temperature, $\theta_{transition}$. θ is the non-dimensional temperature defined in Equation 2 [22].

$$\hat{\theta} \equiv \begin{cases} 0 & for\ \theta < \theta_{transition} \\ (\theta - \theta_{transition})/(\theta_{melt} - \theta_{transition}) & for\ \theta_{transition} \le \theta \le \theta_{melt} \\ 1 & for\ \theta > \theta_{melt} \end{cases} \tag{2}$$

By taking the strain rate dependence assumption the stress, $\bar{\sigma}$ and plastic strain, $\dot{\bar{\varepsilon}}^{pl}$ can be defined in Equation 3 and Equation 4, respectively [22].

DOI: https://doi.org/10.11113/jm.v46.494

$$\bar{\sigma} = \sigma^0\left(\bar{\varepsilon}^{pl}, \theta\right) R\left(\dot{\bar{\varepsilon}}^{pl}\right) \quad (3)$$

$$\dot{\bar{\varepsilon}}^{pl} = \dot{\varepsilon}_0 \exp\left[\frac{1}{C}(R-1)\right] \quad for\ \bar{\sigma} \geq \sigma^0 \quad (4)$$

The relationship can be defined as shown in Equation 5 [22]

$$\bar{\sigma} = \left[A + B\left(\bar{\varepsilon}^{pl}\right)^n\right]\left[1 + C \ln\left(\frac{\dot{\bar{\varepsilon}}^{pl}}{\dot{\varepsilon}_0}\right)\right](1 - \hat{\theta}^m) \quad (5)$$

whereby C and $\dot{\varepsilon}_0$ are the material parameters that can be defined based on Johnson-Cook rate dependencies.

Johnson Cook's damage model or referred to as the "Johnson-Cook dynamic failure model" is suitable only for high-strain-rate deformation of metals and alloys. The Johnson-Cook dynamic failure model is based on the value of the equivalent plastic strain at element integration points; failure is assumed to occur when the damage parameter exceeds 1. The damage parameter, ω, is defined in Equation 6 [22].

$$\omega = \sum\left(\frac{\Delta\bar{\varepsilon}^{pl}}{\bar{\varepsilon}_f^{pl}}\right) \quad (6)$$

where $\Delta\,\bar{\varepsilon}^{\,pl}$ is an increment of the equivalent plastic strain, $\bar{\varepsilon}_f^{pl}$ is the strain at failure. The strain at failure, $\bar{\varepsilon}_f^{pl}$ can be defined as shown in Equation 7 [22].

$$\bar{\varepsilon}_f^{pl} = \left[d_1 + d_2 \exp\left(d_3 \frac{p}{q}\right)\right]\left[1 + d_4 \ln\left(\frac{\dot{\bar{\varepsilon}}^{pl}}{\dot{\varepsilon}_0}\right)\right]\left(1 + d_5\,\hat{\theta}\right) \quad (7)$$

where d_1 (initial failure strain), d_2 (exponential factor), d_3 (triaxiality factor), d_4(strain rate factor), and d_5 (temperature factor) are failure parameters measured at or below the transition temperature, $\theta_{\,transition}$, $\dot{\varepsilon}_0$ is the reference strain rate, p is the pressure stress and q is the Mises stress [22].

2.1.2 Isotropic hardening plasticity model

Isotropic hardening is generally considered to be a suitable model for problems in which the plastic straining goes well beyond the incipient yield state. Isotropic hardening plasticity is written in Equation 8 [22].

$$f(\sigma) = \sigma^0\left(\varepsilon^{pl}, \theta\right) \quad (8)$$

where θ is temperature, σ^0 is the equivalent (uniaxial) stress, ε^{pl} is the work equivalent plastic strain, defined by Equation 9 [22].

$$\sigma^0 \dot{\varepsilon}^{pl} = \sigma : \dot{\varepsilon}^{pl} \quad (9)$$

2.1.3 Ductile damage model and damage evolutions

The ductile damage model is a phenomenological model for predicting the onset of damage due to nucleation, growth, and coalescence of voids. The model assumes that the equivalent plastic strain at the onset of damage, $\dot{\bar{\varepsilon}}_D^{pl}$ is a function of stress triaxiality and strain rate in Equation 10 [22].

$$\bar{\varepsilon}_D^{pl}\left(\eta, \dot{\bar{\varepsilon}}^{pl}\right) \quad (10)$$

where $\eta = p/q$ is the stress triaxiality, p is the pressure stress, q is the Mises equivalent stress, and $\dot{\bar{\varepsilon}}^{pl}$ is the equivalent plastic strain rate. The damage model initiation is met when the following condition in Equation 11 is satisfied [22].

DOI: https://doi.org/10.11113/jm.v46.494

$$\omega_D = \int \frac{d\bar{\varepsilon}^{pl}}{\bar{\varepsilon}_D^{pl}(\eta, \dot{\bar{\varepsilon}}^{pl})} = 1 \tag{11}$$

where ω_D is a state variable that increases monotonically with plastic deformation as shown in Figure 1.

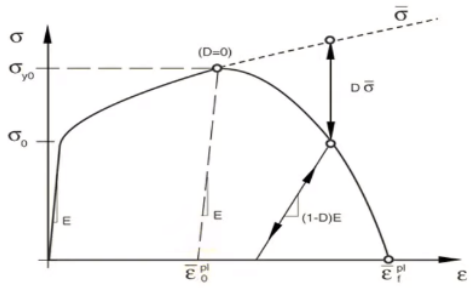

Figure 1: Ductile damage model on the typical strain-stress graph [22]

The equivalent plastic strain at the damage initiation, ε_0^{pl} is determined by offsetting the plastic strain at the ultimate strength strain ductile damage. This will be the value of the fracture strain [22]. The stress triaxiality can be defined as per Equation 12 below based on Table 1;

$$\eta = -\frac{p}{q} = \frac{\frac{1}{3}trace\,(T)}{\sigma_{mises}} = \frac{\frac{1}{3}(\sigma_{xx}+\sigma_{yy}+\sigma_{zz})}{\sigma_{mises}} \tag{12}$$

Table 1: Von Mises yield criterion [23]

State of stress	Boundary conditions	von Mises equations
General	No restrictions	$\sigma_v = \sqrt{\frac{1}{2}\left[(\sigma_{11}-\sigma_{22})^2+(\sigma_{22}-\sigma_{33})^2+(\sigma_{33}-\sigma_{11})^2\right]+3\left(\sigma_{12}^2+\sigma_{23}^2+\sigma_{31}^2\right)}$
Principal stresses	$\sigma_{12}=\sigma_{31}=\sigma_{23}=0$	$\sigma_v = \sqrt{\frac{1}{2}\left[(\sigma_1-\sigma_2)^2+(\sigma_2-\sigma_3)^2+(\sigma_3-\sigma_1)^2\right]}$
General plane stress	$\sigma_3=0$ $\sigma_{31}=\sigma_{23}=0$	$\sigma_v = \sqrt{\sigma_{11}^2-\sigma_{11}\sigma_{22}+\sigma_{22}^2+3\sigma_{12}^2}$
Principal plane stress	$\sigma_3=0$ $\sigma_{12}=\sigma_{31}=\sigma_{23}=0$	$\sigma_v = \sqrt{\sigma_1^2+\sigma_2^2-\sigma_1\sigma_2}$
Pure shear	$\sigma_1=\sigma_2=\sigma_3=0$ $\sigma_{31}=\sigma_{23}=0$	$\sigma_v = \sqrt{3}\lvert\sigma_{12}\rvert$
Uniaxial	$\sigma_2=\sigma_3=0$ $\sigma_{12}=\sigma_{31}=\sigma_{23}=0$	$\sigma_v = \sigma_1$

Damage evolutions define the damage progression after the damage is initiated. It can be determined by energy and displacement damage. By using an energy damage evolution, the fracture energy, G_f is defined as shown in Equation 13 [22],

$$G_f = \int_{\bar{\varepsilon}_0^{pl}}^{\bar{\varepsilon}_f^{pl}} L\sigma_y d\bar{\varepsilon}^{pl} = \int_0^{\bar{u}_f^{pl}} \sigma_y d\bar{u}^{pl} \tag{13}$$

where L is the characteristic length. By using displacement as a damage evolution, the displacement at failure, $\bar{u}_f^{pl}$ can be defined in Equation 14 [22].

$$\bar{u}_f^{pl} = \frac{2G_f}{\sigma_{y0}} \tag{14}$$

DOI: https://doi.org/10.11113/jm.v46.494

2.2 Experimental setup and testing.

Specimen with 250mm (length) x 25mm (width) x 0.29 mm (thickness) of Aluminium Alloy 2024 T3 sheet is prepared for the tensile experiment. The tensile test is performed using Universal Test Machine (UTM) as shown in Figure 2. The tensile test is run with 8mm/minute pulling rate.

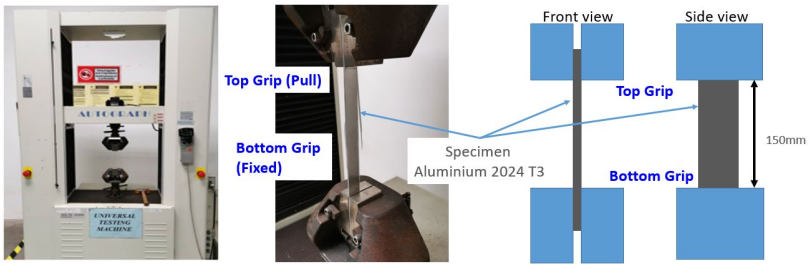

Figure 2: Tensile experiment setup using Universal Test Machine.

2.3 FEM modeling

2.3.1 Modeling in ABAQUS CAE

Aluminium 2024 T3 is modeled as a C3D8R solid element with a mesh size of 0.5mm with 0.29mm thickness. Figure 3 shows the boundary condition of the FEM model, similar to the tensile experimental setup whereby the bottom grip which is used to hold the specimen defined as a fixed boundary condition and the pulling force acted on the top grip is defined as a displacement boundary condition with 8mm per minute pulling rate.

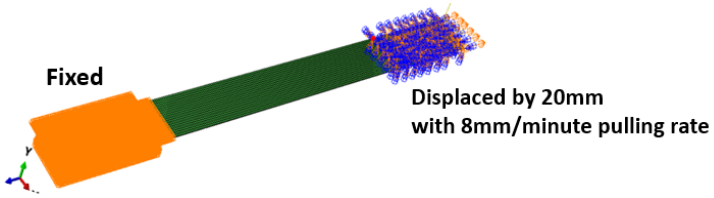

Figure 3: ABAQUS CAE model and boundary conditions.

During the initial modeling, the FEM tensile test is performed without applying the damage properties, and the Aluminium 2024 T3 properties are used based on the literature review from Table 2 and Table 3 with a density value of 2.78g/cm^3 and Young's Modulus value of 73.1GPa [24].

Table 2: Johnson Cook's plasticity model [25]

Parameter	Yield Stress, A (MPa)	Strain hardening modulus, B (MPa)	Strain hardening exponent, *n*	Temperature factor exponent, *m*	Strain rate effect, C
Value	265	426	0.34	1	0.018

Table 3: Isotropic hardening plasticity model [24]

True Stress, σ (MPa)	345.00	386.12	441.31	482.00
Plastic strain, $\dot{\varepsilon}^{pl}$	0.0	0.051	0.128	0.171

The result of the FEM tensile test initial run shows the Aluminium 2024 T3 stress-strain graph using Johnson Cook's model and the isotropic plasticity model are well-fitted with the other literature review data presented in Figure 4.

DOI: https://doi.org/10.11113/jm.v46.494

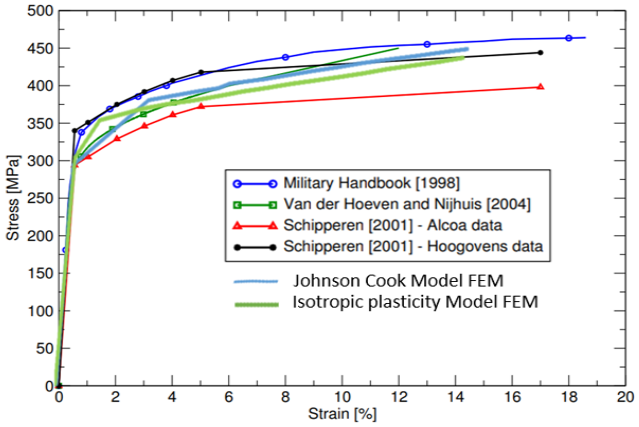

Figure 4: Johnson Cook's FEM model and Isotropic hardening plastic FEM model stress-strain graph using the literature review properties model and comparison with other literature review data [26]

2.3.2 Correlation data between experimental result and FEM modeling

2.3.2.1 Yield stress and ultimate tensile strength determination

Based on the experiment stress-strain graph as shown in Figure 5, Young's Modulus value is only 36.513GPa and it is considered very low for a typical Aluminium 2024 T4 which is 73.1GPa. It is suspected that at the start of the tensile test, there is a slip causing a low value of Young's Modulus.

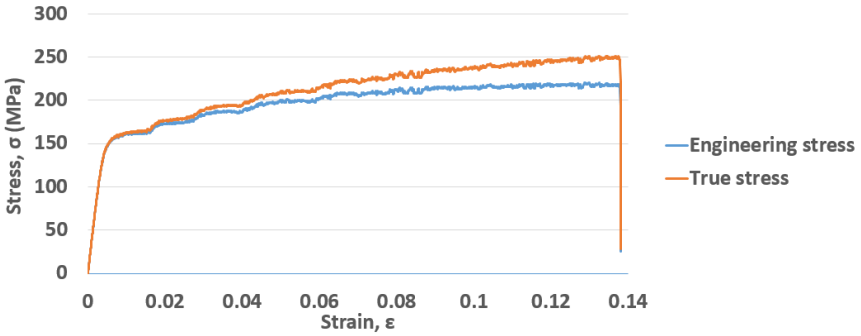

Figure 5: Engineering stress-strain and true stress-strain graph experiment result with 8mm/minute pulling rate.

Therefore, an adjustment had been made at the start of the experiment to accommodate the slip and to meet the typical Aluminium 2024 T3 Young's Modulus value at 73.1GPa as shown in Figure 6. By using the y-value of the experiment data and fit it into the equation, y=73100x at the elastic area, the new adjusted data is created as shown in Figure 7.

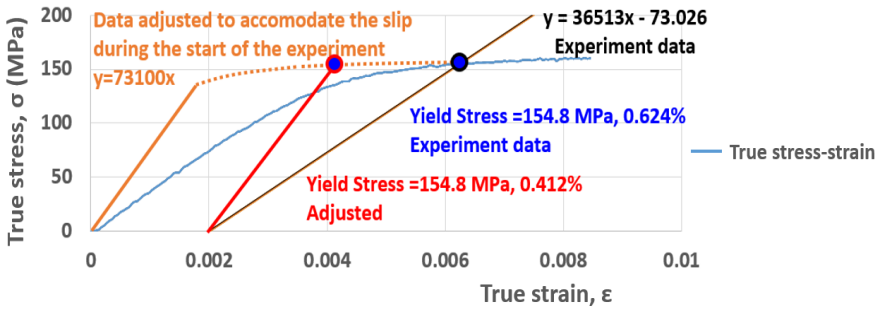

Figure 6: Data adjustment at the start of the experiment to accommodate the slip

DOI: https://doi.org/10.11113/jm.v46.494

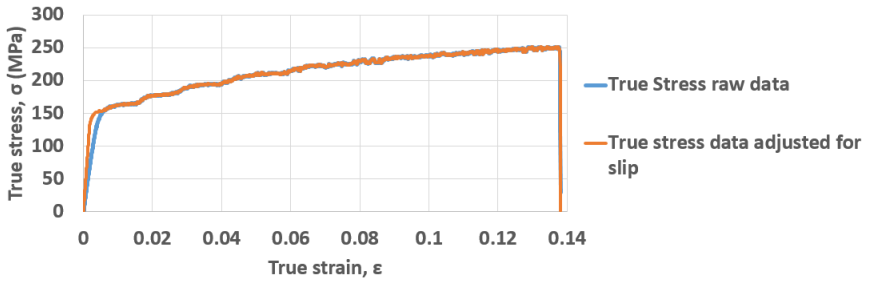

Figure 7: True stress-strain graph before and after data was adjusted to accommodate the slip

Based on Figure 6 and Figure 7 which show the true stress-strain graph before and after the data had been adjusted to accommodate the slip, the yield stress value is 154.8 MPa (0.2% offset of the strain). The ultimate tensile strength is 251.18MPa at 12.97% strain (true stress value at maximum engineering stress, 220.625MPa) determined in Figure 5.

2.3.2.2 Johnson Cook plasticity and damage model parameter determinations

By taking the first portion of Equation 5, the plastic hardening properties without strain rate dependencies can be defined by using Equation 16 with the experiment data.

$$\bar{\sigma} = \left[A + B\left(\bar{\varepsilon}^{pl}\right)^{n}\right] \quad (15), \rightarrow \quad \ln\left(\sigma_y - A\right) = n.\ln(\varepsilon) + \ln(B) \quad (16)$$

By using Equation 16 and experiment result data (true stress, σ_y, yield stress, A and true strain, ε), $\ln\left(\sigma_y - A\right)$ versus ln (ε) is plotted as shown in Figure 8. By taking the significantly straight graph as highlighted in Figure 8, the value of B (strain hardening modulus) and n (strain hardening exponent) can be derived from the linear trend line equations as shown in Figure 8.

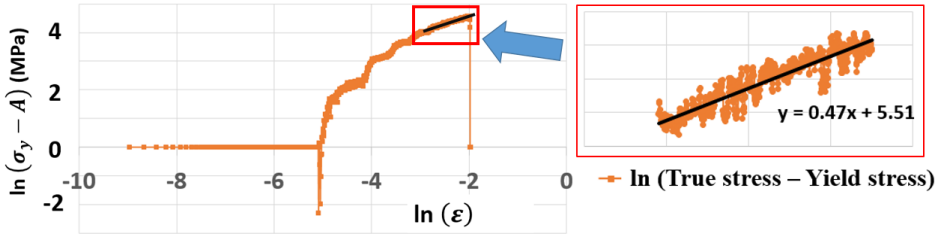

Figure 8: Determination of B and n values from the experiment data

From the linear trend line in Figure 8, the B value is $e^{5.51}$ = 247.15 MPa and n = 0.47. Since experiment test data is unavailable for different strain rates and specimen tests, the literature review Johnson Cook's damage model values are interpolated and estimated as shown in table 4. Data interpolation and estimation are used for modeling purposes only.

Table 4: Johnson Cook's damage model [25] and the interpolated and estimated damage model values used for modeling purposes only

Parameter	d_1	d_2	d_3	d_4	d_5
Johnson Cook's literature damage value	0.13	0.13	-1.5	0.011	0
Johnson Cook's interpolated and estimated damage value	0.06	0.06	-1.0	0.011	0

2.3.2.3 Isotropic plasticity hardening determination

By using the experimental data, the plastic strain was determined based on equation 9 and the results as shown in Table 5.

DOI: https://doi.org/10.11113/jm.v46.494

Table 5: Isotropic hardening plasticity model based on experimental data

True Stress, σ (MPa)	154.80	177.71	199.84	218.79	230.7	239.09	246.55	251.19
Plastic strain, $\dot{\varepsilon}^{pl}$	0.00	0.02	0.04	0.06	0.08	0.10	0.12	0.126

2.3.2.4 Ductile damage model parameter determination

By zooming the true stress-strain graph in Figure 7 at the damaged area (from the ultimate strength point to the fracture point), and offsetting the plastic strain at the ultimate strength strain ductile damage point (251.18MPa at 12.97% strain) by using offsetting line slope value at 73.1GPa (Aluminium 2024 T3 Young Modulus), the fracture strain can be determined as shown in Figure 9. The offset plastic strain value is 0.1263 and this value is the fracture strain or the equivalent plastic strain at the damage initiation, ε_0^{pl}.

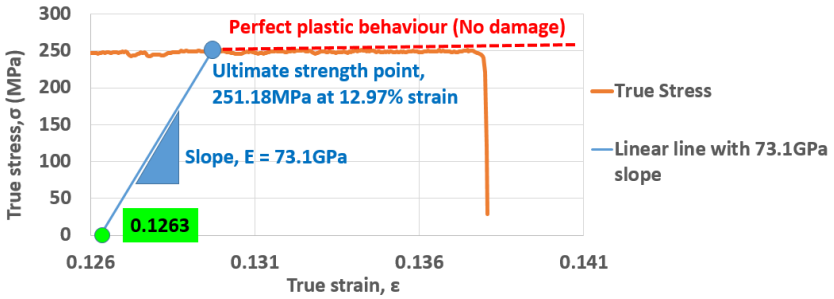

Figure 9: Determination of the fracture strain, ε_0^{pl}

The stress triaxiality, η and the strain rate are assumed to be 0 as no other experiments were performed at different strain rates.

2.3.2.2 Damage evolutions calculation

The first step to define the damage evolutions is to convert the true stress-strain graph to the true strain-plastic displacement graph as presented in Figure 10.

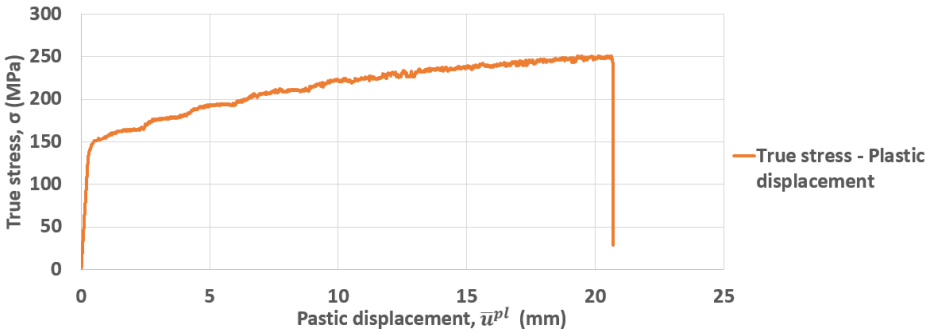

Figure 10: True stress-plastic displacement graph

From Figure 1, the damage, D can be simplified as shown in Equation 17,

$$\sigma = (1 - D).\bar{\sigma} \quad \rightarrow \quad D = -1(\frac{\sigma}{\bar{\sigma}} - 1) \tag{17}$$

where σ is the actual stress at the damage condition and $\bar{\sigma}$ is the stress value at the perfect plastic behavior after the ultimate strength point in reference to actual stress. Next, the true stress-plastic displacement graph is simplified at the damaged area (from the ultimate strength point to the fracture point) by referring to Figure 1 and using Equation 17 as shown in Figure 11 to define the values of the plastic displacement at failure, $\bar{u}_f^{pl}$ and the damage, D.

DOI: https://doi.org/10.11113/jm.v46.494

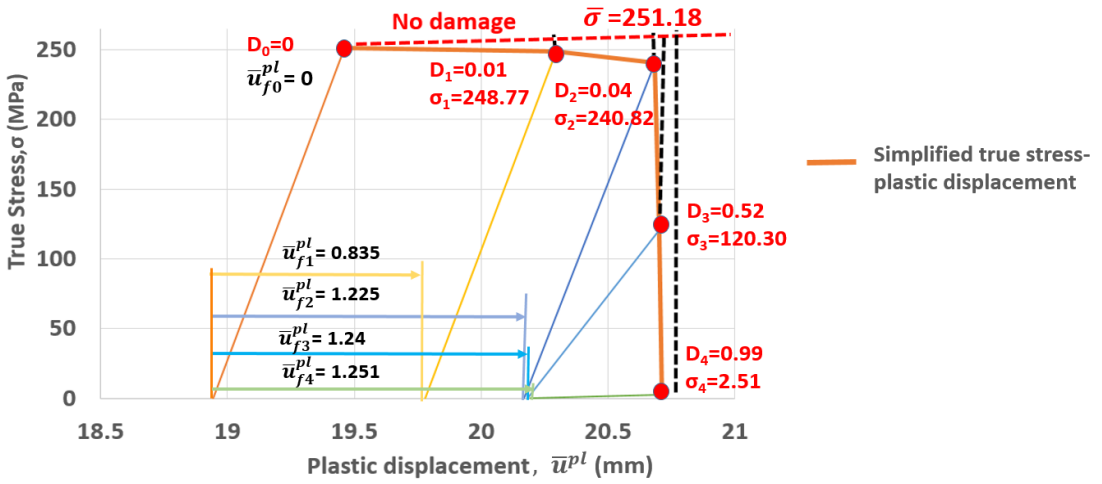

Figure 11: Plastic displacement at failure, $\bar{u}_f^{pl}$ and the damage, D from simplified true stress-plastic displacement graph

By using the damage, D at the respective displacement at failure, $\bar{u}_f^{pl}$ values as shown in Figure 11, the FEM result is still far deviated to the experiment result. Therefore, the plastic displacement at failure is further tweaked by using a damage reference point at 1% or D=0.01 instead of D=0 for a smaller plastic displacement to further improve the deviation to the experiment result. The new plastic displacement at failure and damage are shown in Figure 12.

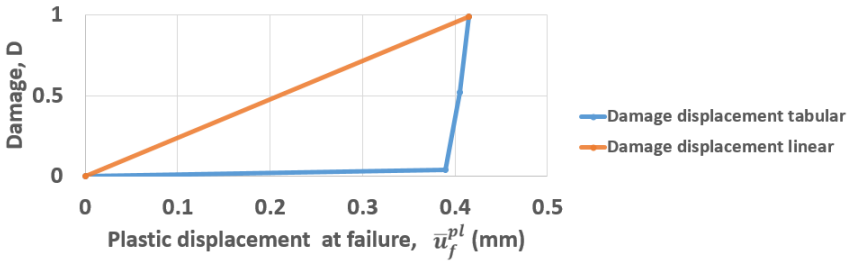

Figure 12: Tweaked plastic displacement at failure, $\bar{u}_f^{pl}$ and the damage, D

With the characteristic length at 0.29mm, by using Equation 14, the fracture energy can be defined using a displacement at failure (linear) at 0.415mm and the value is 52.12 N.mm.

3.0 RESULTS AND DISCUSSION

Based on the comparison with the experiment sample failure mode, both FEM model failure mode is closely identical to the experiment sample failure mode as shown in Figure 13. The comparison of the tensile test stress-strain graph between experiment results, Johnson Cook's FEM model and isotropic plastic with ductile damage FEM model are shown in Figure 14. By looking at the mechanical properties comparison between FEM models with the experiment result presented in Table 6, Johnson Cook's FEM model shows a bigger deviation, which is up to 10.5% deviation compared to the isotropic plastic with ductile damage FEM model, which is only up to 3.3% deviation. Based on the stress analysis comparison of both FEM models presented in Table 6 and Figure 15, the ultimate tensile strength difference is only 0.1% but the yield stress shows higher differences which is 6.9%.

DOI: https://doi.org/10.11113/jm.v46.494

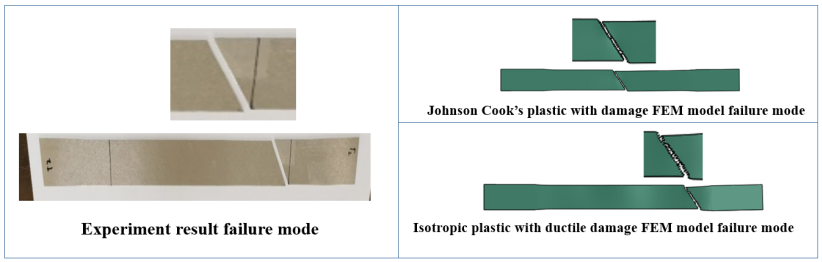

Figure 13. Comparison between the experimental sample and FEM models failure mode

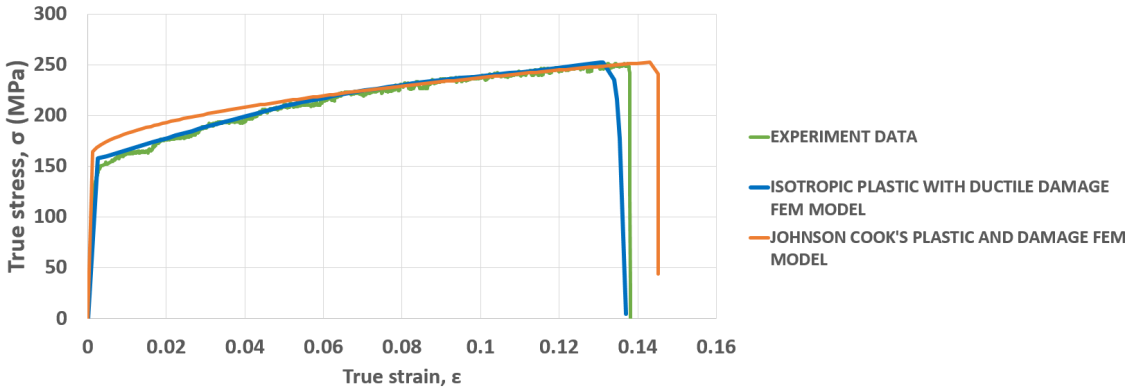

Figure 14: Tensile test true stress-strain comparison between the experiment, Johnson Cook's FEM model and Isotropic plastic with ductile damage FEM model

Table 6: Mechanical properties comparison between experiment, Johnson Cook's FEM model and Isotropic plastic with ductile damage FEM model

Parameter	Experiment value	Johnson Cook's FEM model	Deviation to experiment results	Isotropic plastic with ductile damage FEM model	Deviation to experiment results	FEM models comparison
Yield Stress	154.80 MPa	171.0 MPa	10.5%	160.0 MPa	3.3 %	6.9%
Ultimate tensile strength	251.18 MPa	252.68 MPa	0.6 %	252.37 MPa	0.5 %	0.1%
Ultimate strain	12.97 %	14.32%	10.4 %	13.1 %	0.6 %	9.3%

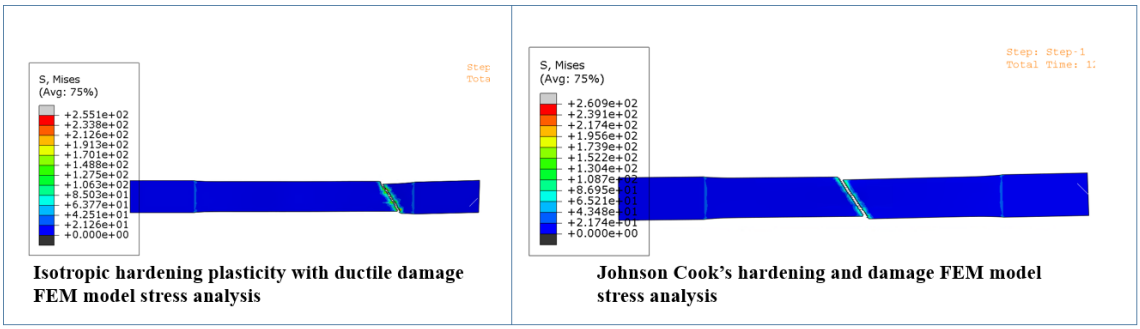

Figure 15: Stress analysis comparison between Johnson Cook's FEM model and isotropic plastic with ductile damage FEM model

The deviation of the yield stress for Johnson Cook's FEM model is relatively high (more than 5%) compared to the experiment result and isotropic plastic FEM model as presented in Table 6. With this, the strain hardening modulus, *B* and strain hardening exponent, *n* obviously needs further tweaks and optimization study and it requires more effort and simulation runs. From a single

DOI: https://doi.org/10.11113/jm.v46.494

experimental stress-strain graph as representative of limited sample data, ductile damage parameters (equivalent fracture strain, stress triaxiality and strain rate) can be defined and calculated. Obviously, a single experiment stress-strain graph cannot be used to define Johnson Cook's damage parameters (initial failure strain, exponential factor, triaxiality factor, strain rate factor and temperature factor). More experiments with different strain rates are required to define Johnson Cook's damage parameters. However, a single experiment might be low in accuracy, therefore more experiments are required for the isotropic hardening plasticity to improve the data accuracy. This is to have the experimental data with different strain rates so that more stress-strain data at different strain rates.

4.0 CONCLUSION

With the limited sample and data, the isotropic plastic hardening with ductile damage FEM model is more appropriate to be used compared to Johnson Cook's FEM model based on the 2 important findings based on this study as below;

i. Johnson Cook's plastic hardening FEM model requires more effort to tweak and optimize the strain hardening modulus and strain hardening exponent to match the experiment result.
ii. From a single experimental stress-strain graph, the ductile damage parameters can be defined and calculated but it cannot be used to define Johnson Cook's model damage parameters. Johnson Cook's damage parameters determination requires more experiments with different strain rates.

ACKNOWLEDGMENTS

This project is funded by the Ministry of Higher Education (MOHE) of Malaysia, ref no. FRGS/1/2018/TK03/UiTM/02/5. Thank you to Universiti Teknologi MARA (UiTM), Malaysia for various and generous assistance throughout the project until completion.

REFERENCES

1. Ahmad S.A, et al., *Finite Element Modelling of Aluminum Alloy 2024-T3 under Transverse Impact Loading.* AIP Conference Proceedings Vol. 1901, 2017 **050005**.
2. Shuaishuai Y. et. al., *A modified Johnson-Cook model of AA6061-O aluminum alloy with quasi-static pre-strain at high strain rates* International Journal of Material Forming 2021 **14**, pp. 677–689.
3. Zhang D. N. et al., *A modified Johnson–Cook model of dynamic tensile behaviors for 7075-T6 aluminum alloy* Journal of Alloys and Compounds, 2015 **619** pp. 186-194.
4. Sachin G., et. al., *Determination of Johnson–Cook Parameters for Cast Aluminum Alloys* Journal of Engineerig Materials and Technology 2014 **136**(3) pp. 034502 (1-4)
5. Tan J. Q., et. al., *A modified Johnson–Cook model for tensile flow behaviors of 7050-T7451 aluminum alloy at high strain rates* Materials Science and Engineering 2015 **631** pp. 214-219.
6. Sohail A., et. al., *Numerical and experimental investigation of Johnson–Cook material models for aluminum (Al 6061-T6) alloy using orthogonal machining approach* Advances in Mechanical Engineering 2018, **10**(9) pp. 1–14.
7. Li S.Y., et. al, *Optimization of Milling Aluminum Alloy 6061-T6 using Modified Johnson-Cook Model* Simulation Modelling Practice and Theory 2021 **111** 102330.
8. Corona, et.al., *An evaluation of the Johnson-Cook model to simulate puncture of 7075 aluminum plates*. Technical report OSTI United States Department of Energy: 2014. **1204105** SAND2014-1550 505013.
9. Rasaee S. et. al., *Constitutive Modeling of 2024 Aluminum Alloy Based on the Johnson–Cook Model* Transactions of the Indian Institute of Metals 2019 **72**, pp. 1023–1030.
10. Kay, G. *Failure Modeling of Titanium-6Al-4V and 2024-T3 Aluminum with the Johnson-Cook Material Model*. Technical report OSTI United States Department of Energy: 2002. **15006359** UCRL-ID-149880.
11. Shen W. J. et. al., *Study on constitutive relationship of 6061 aluminum alloy based on Johnson-Cook model* Materials Today: Communications 2023 **37** 106982.
12. Wang, C., et al., *A modified Johnson–Cook model for 2A12 aluminum alloys*. Mech Time-Depend Mater 2023
13. Bal B. et al., *The Precise Determination of the Johnson–Cook Material and Damage Model Parameters and Mechanical Properties of an Aluminum 7068-T651 Alloy* J. Eng. Mater. Technol. 2019, **141**(4): pp. 041001(1-2-10)

 DOI: https://doi.org/10.11113/jm.v46.494

14. Sonika S., et. al., Finite element analysis of AA1100 elasto-plastic behaviour using Johnson-Cook model Materials Today: Proceeding 2018 **5**(2), pp. 5349-5353
15. Meng X.X., et.al., *An Improved Johnson–Cook Constitutive Model and Its Experiment Validation on Cutting Force of ADC12 Aluminum Alloy During High-Speed Milling* Metals 2020 **10**(8), 1038.
16. Børvik T. et. al., *Empty and foam-filled circular aluminium tubes subjected to axial and oblique quasistatic loading* International Journal of Crashworthiness, 2003 **8**(5) pp. 481-494.
17. Ivaylo N. V., et. al., *Anisotropic finite elastoplasticity with nonlinear kinematic and isotropic hardening and application to sheet metal forming* International Journal of Plasticity 2010 26(5) pp. 659-687.
18. Asle J.T., et. al., *Effects of constituent particle content on ductile fracture in isotropic and anisotropic 6000-series aluminium alloys* Materials Science and Engineering: A 2021 **820** 141420.
19. Fribourg G., et.al., *Microstructure-based modelling of isotropic and kinematic strain hardening in a precipitation-hardened aluminium alloy* Acta Materialia 2011 **59**(9) pp 3621-3635
20. Ole R. M., et. al., *Nanoscale modelling of combined isotropic and kinematic hardening of 6000 series aluminium alloys* Mechanics of Materials 2020 **151** 103603
21. Abir B. et. al., *Experimental and numerical methodology to characterize 5083-aluminium behavior considering non-associated plasticity model coupled with isotropic ductile damage* International Journal of Solids and Structures 2021 **229** 111139.
22. *ABAQUS CAE user manual*. [Internet Reference]. Available from: https://classes.engineering.wustl.edu/2009/spring/mase5513/abaqus/docs/v6.6
23. *Von_Mises_yield_criterion.* [Internet Reference]. Available from: https://en.wikipedia.org/wiki/Von_Mises_yield_criterion
24. *ASM Aerospace Specification Metals-Aluminium 2024 T3.* [Internet Reference]. Available from: http://asm.matweb.com/search/SpecificMaterial.asp?bassnum=MA2024T3
25. Johnson, G.R. et al, *A constitutive model and data for metals subjected to large strains, high strain rates and high temperatures.* 7th International Symposium on Ballistics. 1983.
26. M.Hagenbeek. *Characterization of the Fiber Metal Laminates under Thermo-mechanical loadings.* Doctorate dissertation. Delft University of Technology 2005.

 DOI: https://doi.org/10.11113/jm.v46.494